CA). Mismatch primer pairs (sense: 5′-tgctgggattacagatgtgag-3′; antisense: 5′-tgcaaaccaatcagaattcatg-3′) were prepared for PCR-RFLP analysis to generate the *Bsp*HI site (tcatga) in a mutant allele. *Bsp*HI was used to digest the 200-bp mutant (c.1175C>T) PCR product, which generated the 178-bp PCR product.

Enzyme Assay

Mitochondrial LCKT activity in lymphoblastoid cells from the two patients and from two healthy adult males (as the control) was determined using 10 μM 2-ketopalmitoyl-CoA as a substrate [Purevsuren et al., 2009]. Citrate synthase activity was determined spectrophotometrically using DTNB.

MTP Expression Analysis

Cell extracts of lymphoblastoid cells from Patients IV-1 and IV-2 and two healthy adult males and of MTP-deficient fibroblasts (previously reported by Purevsuren et al. [2009]) were subjected to 12.5% sodium dodecyl sulfate-polyacrylamide gel electrophoresis (SDS-PAGE). Western blot analysis was performed using a rabbit polyclonal antibody specific for both the α- and β-subunits of MTP or medium-chain acyl-CoA dehydrogenase (MCAD) (both antibodies were generously provided by Dr. T. Hashimoto, Professor Emeritus, Shinshu University), and blots were visualized using the Immuno-Pure NBT/BCIP Substrate Kit (Promega, Madison, WI).

Construction of Wild-Type and Mutant HADHB-FLAG and Wild-Type HADHA-MYC Expression Vectors

The wild-type HADHB expression vector was prepared by subcloning *HADHB* cDNA at the *Not*I/*Eco*RV site of a mammalian expression vector, p3 × FLAG-CMV (Sigma–Aldrich, St. Louis, MO) (pHADHB-FLAG). An *Eco*RV recognition site (gatatc) was introduced at the termination codon (TAA) of *HADHB*. The mutant *HADHB* (pHADHB-A392V-FLAG, pHADHB-R61C-FLAG, pHADHB-N389D-FLAG, and pHADHB-R444K-FLAG; amino acid number is shown from the first methionine) and the wild-type *HADHA* (pHADHA-MYC) expression vectors were prepared using the in vitro mutagenesis method [Yamada et al., 2013]. The generated expression vectors encoded the FLAG-tagged wild-type or mutant β-subunits and MYC-tagged α-subunit protein at the *C*-terminus.

Analysis of the Association of the Wild-Type or Mutant β-Subunits With the Wild-Type α-Subunit

Various combinations of 0.4 μg of wild-type or mutant HADHB-FLAG expression vectors and 0.4 μg of the HADHA-MYC expression vector were co-transfected into HEK293 cells in 24-well dishes using Lipofectamine 2000 reagent (Life Technologies, Carlsbad, CA). Sixty hours after transfection, the cells were collected, and the extracts were subjected to immunoprecipitation using anti-FLAG M2 antibody-conjugated agarose (Sigma–Aldrich) for 2 hr at 4°C with gentle mixing [Yamada et al., 2013]. After washing the gels, the precipitates were subjected to a 10% SDS-PAGE, and proteins were transferred to a PVDF membrane (Immobilon-P). Western blot analysis was performed with anti-FLAG M2 antibody (for the β-subunit) and with anti-MYC antibody (for the α-subunit, kindly provided by Dr. K. Nagata, Aichi Human Service Center). Immunoreactive bands were visualized with an enhanced chemiluminescence western blotting detection system (GE Healthcare, Waukesha, WI).

Structural Analysis of MTP

A homology model of human MTP was built using the Swiss-Model automated modeling server [Kiefer et al., 2009]. N389 and A392 of the β-subunit of the MTP coordinate (PDB code: 1wdk) [Ishikawa et al., 2004] were replaced with aspartate (D) and valine (V), respectively, using the Swiss PDB Viewer [Guex and Peitsch, 1997] to determine the effect of these substitutions on the surrounding residues.

RESULTS

Identification of the Mutation

The nucleotide sequences of all exons and splice sites of the candidate genes of autosomal recessive isolated hypoparathyroidism, *PTH* and *GCMB*, revealed no mutations. Since mutations of *HADHA* and *HADHB* cause rhabdomyolysis in infancy, we determined the nucleotide sequences of all exons and intron-exon boundaries of the genes from the patients and identified a homozygous mutation (c.1175C>T, [p.A392V]) in exon 14 of *HADHB* (NM_000183) (the first methionine is numbered as one) (Fig. 1C). PCR-RFLP analysis demonstrated that the patients were homozygous, whereas the parents and grandmother were heterozygous for the mutation (Fig. 1D). The mutation was absent in 200 normal alleles.

A392V in the β-Subunit Causes MTP Deficiency

The LCKT activities of the lymphoblastoid cells of the Patients IV-1 and IV-2 were decreased to 5% and 14% of normal controls, respectively (Fig. 2A). Western blot analysis showed faint or no bands for the α- and β-subunits bands of MTP from the patient's lymphoblastoid cells. In contrast, both subunits were clearly detected in control lymphoblastoid cells (Fig. 2B). Thus, the patients were found to have MTP deficiency caused by decreased amounts of α- and β-subunits.

The A392V β-Subunit Does Not Associate With the α-Subunit of MTP

Hetero-octamer formation of the four α- and four β-subunits is necessary for MTP activity. To confirm the MTP deficiency evaluated by the enzyme assay and western blot analysis, we studied the effect of mutant β-subunits on the formation of the MTP hetero-octamer with the α-subunit by immunoprecipitation. Western blot

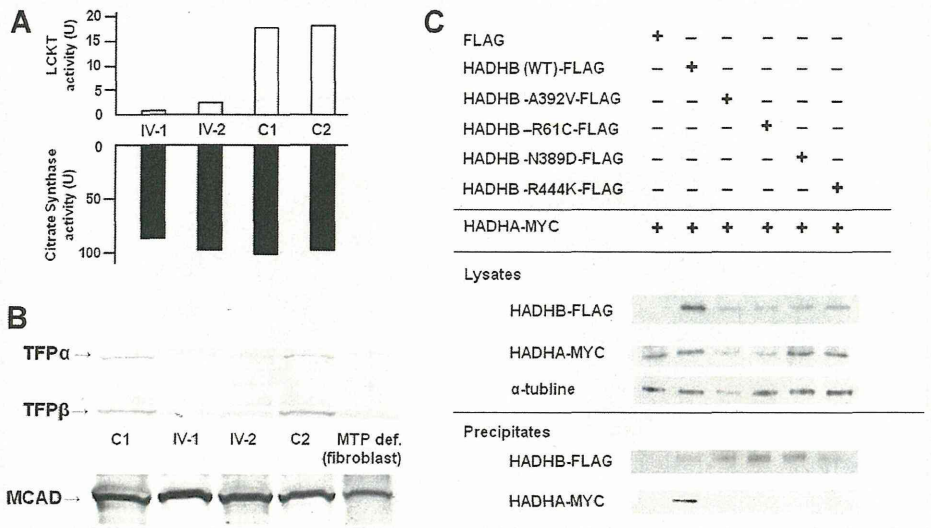

FIG. 2. Biochemical analyses of the MTP protein of the patients. A: The LCKT activities [upper panel] and citrate synthase activities [lower panel] in lymphoblastoid cells from the patients and two controls are shown [1U = μmol/min/mg protein]. B: Western blot analysis of the α- and β-subunits of MTP and MCAD protein [EC 1.3.99.3] [positive control] from the patients and controls lymphoblastoid cells and MTP-deficient fibroblasts are shown. C: Immunoprecipitation of the wild-type or mutant β-subunits with the wild-type α-subunit. [+] Indicates the FLAG- or MYC-tagged vectors used in each study. Lysates and precipitates were immunoblotted with antibodies as indicated [FLAG, MYC, and α-tubulin]. The results of western blot analysis are shown.

analysis revealed that expressions of the mutant β-subunit proteins were decreased in HEK293 cells (Fig. 2C, Lysates), but were efficiently precipitated (Fig. 2C, Precipitates). The MYC-tagged α-subunit co-precipitated with the FLAG-tagged wild-type β-subunit, whereas less than detectable levels of the α-subunit co-precipitated with the four mutant β-subunits (Fig. 2C). Thus, the A392V mutation, as well as the β-subunit N389D mutation previously reported as being associated with a hypoparathyroidism phenotype, abolished the formation of the MTP hetero-octamer, similar to other β-subunit mutations such as R61C (previously described as R28C; lethal phenotype) and R444K (previously described as R411K; neuromyopathic phenotype) [Spiekerkoetter et al., 2003; Purevsuren et al., 2009].

N389D and A392V Mutations Affect the Conformation of the β-Subunit

We analyzed a homology model of the β-subunit of human MTP. N389 and A392 of human MTP are located on the solvent-exposed surface of tetrameric MTP (Fig. 3A). These data indicated that N389 and A392 are not involved in the intersubunit interaction. The catalytic triad, composed of C138, H428, and C458 (shown as blue letters), is located very close to N389 and A392 in the homology model of human MTP (Fig. 3B). Moreover, N389 and A392 are both located on the Cα2 helix in the homology model and directly interact with the Cα1 helix. Notably, the hydrogen bond between the side chains of D389 and T356 is missing in the N389D human MTP model (Fig. 3B,C), and a slight steric clash exists between the side chains of V392 and T356 in the A392V mutant model (Fig. 3D).

DISCUSSION

MTP deficiency caused by mutations of *HADHA* or *HADHB* has been classified into three clinical phenotypes: a lethal phenotype with neonatal onset (severe form), a hepatic phenotype with infantile onset (intermediate form), and a neuromyopathic phenotype with late-adolescent onset (mild form) [Spiekerkoetter et al., 2003]. The clinical features of the patients, together with their decreased LCKT activities, the decreased protein levels of both α- and β-subunits in the patients' lymphoblastoid cells, and the failure of the mutant β-subunit to form an active hetero-octamer with the wild-type α-subunit of the MTP protein indicate that the patients presented in this study have the neuromyopathic phenotype of MTP deficiency due to a homozygous A392V mutation in *HADHB*. Spiekerkoetter et al. [2004] reported that the neuromyopathic phenotype is the major phenotype of MTP deficiency. In contrast, only two of six Japanese cases reported in the literature have presented with the neuromyopathic phenotype [Purevsuren et al., 2009; Yagi et al., 2011]. The fact that the number of cases reported with the neuromyopathic phenotype in Japan is small is most likely because this phenotype is included in the differential diagnosis of early or late-adolescent onset CMT disease with or without episodic myoglobinuria [Spiekerkoetter et al., 2004].

Only two cases of MTP deficiency associated with hypoparathyroidism have been reported (Table I). Dionisi-Vici et al. [1996] first

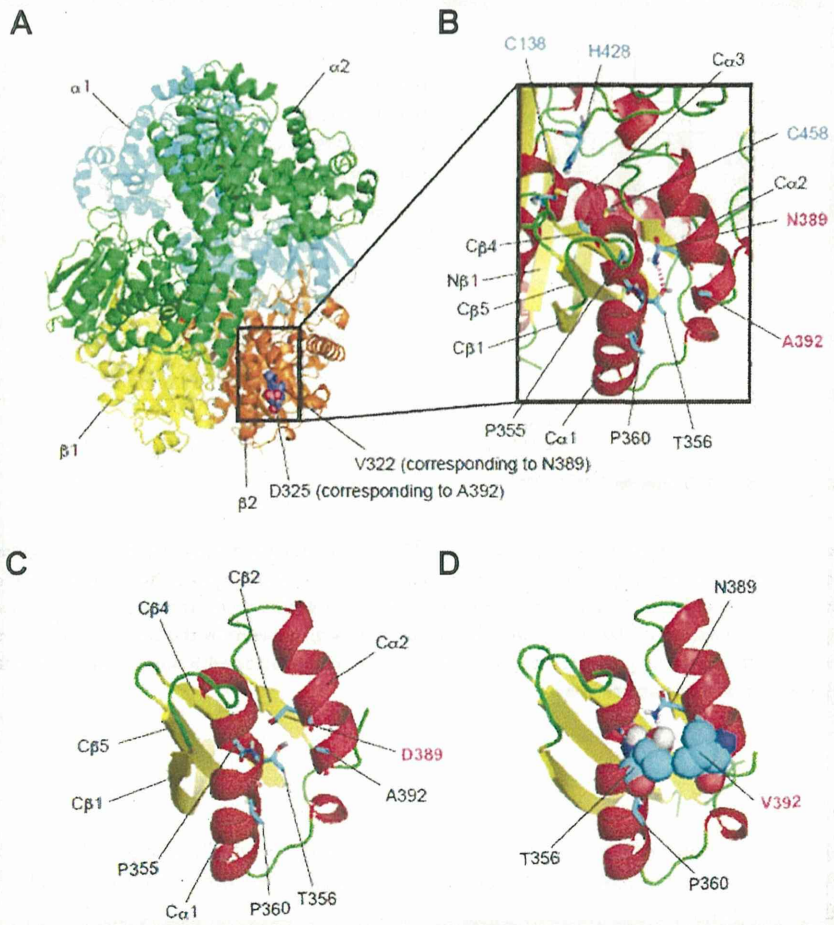

FIG. 3. Structure and homology modeling of MTP. A: α2β2 tetrameric structure of MTP. Molecules colored in cyan and green are the α-subunits [α1 and α2, respectively] of MTP from *Pseudomonas fragi*, whereas those colored in yellow and orange are the β-subunits [β1 and β2, respectively] [Ishikawa et al., 2004]. V322 and D325 are depicted as sphere models. These residues correspond to N389 and A392 of human MTP. B: Enlarged view of the homology model of one of the β-subunits of human MTP. α-helices and β-strands are colored in red and yellow, respectively. Hydrogen, carbon, oxygen, nitrogen, and sulfur atoms are colored in gray, cyan, red, blue, and yellow, respectively. Secondary structure nomenclature [Nβ1, Cβ1, Cβ4, Cβ5, Cα1, Cα2, and Cα3] defined in the yeast thiolase structure [Mathieu et al., 1997] is also indicated. Helices corresponding to Lα1 [171–175], Lα2, and Lα3 of yeast thiolase [V171-L260] have been removed for clarity. A hydrogen bond between the amino group of N389 and the hydroxyl group of T356 is depicted as a dotted line [pink]. C: View around the N389D mutation in the homology model of the β-subunit of human MTP. D: View around the A392V mutation. T356 and V392 are depicted as sphere models.

reported the case of a female patient with MTP deficiency and hypoparathyroidism. Hypoparathyroidism became apparent when she was admitted to the hospital because of fasting-induced rhabdomyolysis at 15 months of age. She had severe hypotonia, respiratory failure, and peripheral polyneuropathy without renal failure. Her serum iPTH concentration was low (4 pg/ml) with severe hypocalcemia (0.95 mmol/L), and the enzyme activities of MTP in the fibroblasts were all reduced: LCKT activity was absent, and LCHAD and LCEH activities were 30% and 52% of the control mean, respectively. These results indicate that she had MTP deficiency with a neuromyopathic phenotype, caused possibly by an *HADHB* mutation encoding LCKT. Labarthe et al. [2006] also reported a female case with hypoparathyroidism and MTP deficiency caused by a *HADHB* mutation. Hypoparathyroidism (iPTH <5 pg/ml) and severe hypocalcemia (1.2 mmol/L) became evident when she was 4 months old. A homozygous mutation (c.1165A>G, [p.N389D]) in *HADHB* was identified. Her serum iPTH concentration reached normal levels after vitamin D therapy, although she developed peripheral polyneuropathy with decreased nerve conduction velocity. LCKT activity was not reported, but numerous episodes of fasting-induced rhabdomyolysis suggested that she had a defective β-subunit of MTP. Indeed, we demonstrated that the N389D β-subunit does not associate with the wild-type α-subunit (Fig. 2C). Taken together, the sibling patients presented here and the two previously reported cases have similar clinical features of infantile onset hypoparathyroidism, peripheral polyneuropathy, and rhabdomyolysis.

A dysfunction in mitochondrial energy metabolism and/or toxicity of accumulated long-chain fatty acids in the parathyroid glands may have contributed to the pathogenesis of hypoparathyroidism in the patients with MTP deficiency [Saudubray et al., 1999]. In fact, hypoparathyroidism has also been reported in other disorders of mitochondrial fatty acid oxidation, including LCHAD deficiency [Tyni et al., 1997] and MCAD deficiency [Baruteau et al., 2009]. However, this hypothesis cannot explain why hypoparathyroidism has not been reported in patients with the most common inborn mitochondrial fatty acid β-oxidation disorders of carnitine palmitoyl transferase II and very-long-chain acyl-CoA dehydrogenase deficiencies or the severe form of MTP deficiency (a lethal phenotype). Thus, the mechanisms underlying the pathogenesis of the disease presented here remains to be elucidated. Tyni et al. [1997] reported the autopsy findings of a patient with hypoparathyroidism and LCHAD deficiency where the parathyroid glands were severely hypoplastic. These findings suggest that mutations of the proteins associated with β-oxidation cause hypoparathyroidism by congenital malformations of parathyroid glands.

Our studies demonstrate decreased expression of the mutant β-subunits (N389D and A392V) and a failure of those subunits to associate with the wild-type α-subunit (Fig. 2). Moreover, N389D and A392V are located close to the active site and are likely have an immediate impact on the structure and function of the catalytic core of human MTP (Fig. 3C,D). A recent study demonstrated that the β-subunit of MTP interacts and colocalizes with the estrogen receptor α or β in the mitochondria and suggested an important role of the β-subunit in estrogen-mediated lipid metabolism [Zhou et al., 2012a,b]. From this perspective, mutant N389D and A392V β-subunits may cause mitochondria dysfunction, including MTP deficiency due to a failure to associate with the α-subunit of MTP and other proteins that result in dysfunction of parathyroid glands. Further case studies are required to determine whether the specific mutations located in the proximity of the active site of the β-subunit are associated with hypoparathyroidism and MTP deficiency.

Early diagnosis and treatment are important for patients with the neuromyopathic phenotype of MTP deficiency, since peripheral polyneuropathy is progressive [Spiekerkoetter et al., 2004; Yamaguchi et al., 2012]. Our study has demonstrated that MTP deficiency should be considered when patients have hypoparathyroidism as the initial presenting feature in infancy.

ACKNOWLEDGMENTS

We would like to thank the patients and their family members who participated in this study. This work was supported by the Takeda Science Foundation, a Health Labor Sciences Research Grant, and a grant (#21390319) from the Ministry of Education, Culture, Sports, Science, and Technology of Japan to N.W.

REFERENCES

Baruteau J, Levade T, Redonnet-Vernhet I, Mesli S, Bloom MC, Broué P. 2009. Hypoketotic hypoglycemia with myolysis and hypoparathyroidism: An unusual association in medium chain acyl-CoA desydrogenase deficiency (MCADD). J Pediatr Endocrinol Metab 22:1175–1177.

Ding C, Buckingham B, Levine MA. 2001. Familial isolated hypoparathyroidism caused by a mutation in the gene for the transcription factor GCMB. J Clin Invest 108:1215–1220.

Dionisi-Vici C, Garavaglia B, Burlina AB, Bertini E, Saponara I, Sabetta G, Taroni F. 1996. Hypoparathyroidism in mitochondrial trifunctional protein deficiency. J Pediatr 129:159–162.

Guex N, Peitsch MC. 1997. SWISS-MODEL and the Swiss-PdbViewer: An environment for comparative protein modeling. Electrophoresis 18:2714–2723.

IJlst L, Wanders RJA, Ushikubo S, Kamijo T, Hashimoto T. 1994. Molecular basis of long-chain 3-hydroxyacyl-CoA dehydrogenase deficiency: Identification of the major disease-causing mutation in the alpha-subunit of the mitochondrial trifunctional protein. Biochim Biophys Acta 1215:347–350.

Ishikawa M, Tsuchiya D, Oyama T, Tsunaka Y, Morikawa K. 2004. Structural basis for channelling mechanism of a fatty acid beta-oxidation multienzyme complex. EMBO J 23:2745–2754.

Kiefer F, Arnold K, Künzli M, Bordoli L, Schwede T. 2009. The SWISS-MODEL Repository and associated resources. Nucleic Acids Res 37: D387–D392.

Labarthe F, Benoist JF, Brivet M, Vianey-Saban C, Despert F, de Baulny HO. 2006. Partial hypoparathyroidism associated with mitochondrial trifunctional protein deficiency. Eur J Pediatr 165:389–391.

Mathieu M, Modis Y, Zeelen JP, Engel CK, Abagyan RA, Ahlberg A, Rasmussen B, Lamzin VS, Kunau WH, Wierenga RK. 1997. The 1.8 A crystal structure of the dimeric peroxisomal 3-ketoacyl-CoA thiolase of *Saccharomyces cerevisiae*: Implications for substrate binding and reaction mechanism. J Mol Biol 273:714–728.

Nakamura Y, Matsumoto T, Tamakoshi A, Kawamura T, Seino Y, Kasuga M, Yanagawa H, Ohno Y. 2000. Prevalence of idiopathic hypoparathyroidism and pseudohypoparathyroidism in Japan. J Epidemiol 10: 29–33.

Parkinson DB, Thakker RV. 1992. A donor splice site mutation in the parathyroid hormone gene is associated with autosomal recessive hypoparathyroidism. Nat Genet 1:149–152.

Purevsuren J, Fukao T, Hasegawa Y, Kobayashi H, Li H, Mushimoto Y, Fukuda S, Yamaguchi S. 2009. Clinical and molecular aspects of Japanese patients with mitochondrial trifunctional protein deficiency. Mol Genet Metab 98:372–377.

Saudubray JM, Martin D, de Lonlay P, Touati G, Poggi-Travert F, Bonnet D, Jouvet P, Boutron M, Slama A, Vianey-Saban C, Bonnefont JP, Rabier D, Kamoun P, Brivet M. 1999. Recognition and management of fatty acid oxidation defects: A series of 107 patients. J Inherit Metab Dis 22: 488–502.

Spiekerkoetter U, Sun B, Khuchua Z, Bennett MJ, Strauss AW. 2003. Molecular and phenotypic heterogeneity in mitochondrial trifunctional protein deficiency due to beta-subunit mutations. Hum Mutat 21: 598–607.

Spiekerkoetter U, Bennett MJ, Ben-Zeev B, Strauss AW, Tein I. 2004. Peripheral neuropathy, episodic myoglobinuria, and respiratory failure in deficiency of the mitochondrial trifunctional protein. Muscle Nerve 29:66–72.

Tyni T, Rapola J, Palotie A, Pihko H. 1997. Hypoparathyroidism in a patient with long-chain 3-hydroxyacyl-coenzyme A dehydrogenase deficiency caused by the G1528C mutation. J Pediatr 131:766–768.

Uchida Y, Izai K, Orii T, Hashimoto T. 1992. Novel fatty acid beta-oxidation enzymes in rat liver mitochondria. II. Purification and prop-

erties of enoyl-coenzyme A (CoA) hydratase/3-hydroxyacyl-CoA dehydrogenase/3-ketoacyl-CoA thiolase trifunctional protein. J Biol Chem 267:1034–1041.

Wanders RJ, Vreken P, den Boer ME, Wijburg FA, van Gennip AH, IJlst L. 1999. Disorders of mitochondrial fatty acyl-CoA beta-oxidation. J Inherit Metab Dis 22:442–487.

Yagi M, Lee T, Awano H, Tsuji M, Tajima G, Kobayashi H, Hasegawa Y, Yamaguchi S, Takeshima Y, Matsuo M. 2011. A patient with mitochondrial trifunctional protein deficiency due to the mutations in the HADHB gene showed recurrent myalgia since early childhood and was diagnosed in adolescence. Mol Genet Metab 104:556–559.

Yamada K, Takado Y, Kato YS, Yamada Y, Ishiguro H, Wakamatsu N. 2013. Characterization of the mutant β-subunit of β-hexosaminidase for dimer formation responsible for the adult form of Sandhoff disease with the motor neuron disease phenotype. J Biochem 153:111–119.

Yamaguchi S, Li H, Purevsuren J, Yamada K, Furui M, Takahashi T, Mushimoto Y, Kobayashi H, Hasegawa Y, Taketani T, Fukao T, Fukuda S. 2012. Bezafibrate can be a new treatment option for mitochondrial fatty acid oxidation disorders: Evaluation by in vitro probe acylcarnitine assay. Mol Genet Metab 107:87–91.

Zhou Z, Zhou J, Du Y. 2012a. Estrogen receptor beta interacts and colocalizes with HADHB in mitochondria. Biochem Biophys Res Commun 427:305–308.

Zhou Z, Zhou J, Du Y. 2012b. Estrogen receptor alpha interacts with mitochondrial protein HADHB and affects beta-oxidation activity. Mol Cell Proteomics 11:M111.011056.

Biochemical and Biophysical Research Communications 448 (2014) 175–181

Contents lists available at ScienceDirect

Biochemical and Biophysical Research Communications

journal homepage: www.elsevier.com/locate/ybbrc

Functional analysis of iPSC-derived myocytes from a patient with carnitine palmitoyltransferase II deficiency

Tetsuhiko Yasuno [a,*], Kenji Osafune [b], Hidetoshi Sakurai [b], Isao Asaka [b], Akihito Tanaka [b], Seiji Yamaguchi [c], Kenji Yamada [c], Hirofumi Hitomi [b], Sayaka Arai [b], Yuko Kurose [b], Yasuki Higaki [d], Mizuki Sudo [d], Soichi Ando [d], Hitoshi Nakashima [a], Takao Saito [a,e], Hidetoshi Kaneoka [a,f]

[a] Division of Nephrology and Rheumatology, Department of Internal Medicine, Fukuoka University School of Medicine, Fukuoka, Japan
[b] Center for iPS Cell Research and Application (CiRA), Kyoto University, Kyoto, Japan
[c] Department of Pediatrics, Shimane University School of Medicine, Izumo, Shimane, Japan
[d] Faculty of Sports and Health Science, Fukuoka University, Japan
[e] General Medical Research Center, Fukuoka University School of Medicine, Japan
[f] Division of Medical Sciences, Fukuoka University School of Nursing, Japan

ARTICLE INFO

Article history:
Received 13 April 2014
Available online 26 April 2014

Keywords:
Carnitine palmitoyltransferase II deficiency
iPSC
Disease modeling
Rhabdomyolysis
Bezafibrate

ABSTRACT

Introduction: Carnitine palmitoyltransferase II (CPT II) deficiency is an inherited disorder involving β-oxidation of long-chain fatty acids (FAO), which leads to rhabdomyolysis and subsequent acute renal failure. The detailed mechanisms of disease pathogenesis remain unknown; however, the availability of relevant human cell types for investigation, such as skeletal muscle cells, is limited, and the development of novel disease models is required.

Methods: We generated human induced pluripotent stem cells (hiPSCs) from skin fibroblasts of a Japanese patient with CPT II deficiency. Mature myocytes were differentiated from the patient-derived hiPSCs by introducing myogenic differentiation 1 (*MYOD1*), the master transcriptional regulator of myocyte differentiation. Using an *in vitro* acylcarnitine profiling assay, we investigated the effects of a hypolipidemic drug, bezafibrate, and heat stress on mitochondrial FAO in CPT II-deficient myocytes and controls.

Results: CPT II-deficient myocytes accumulated more palmitoylcarnitine (C16) than did control myocytes. Heat stress, induced by incubation at 38 °C, leads to a robust increase of C16 in CPT II-deficient myocytes, but not in controls. Bezafibrate reduced the amount of C16 in control and CPT II-deficient myocytes.

Discussion: In this study, we induced differentiation of CPT II-deficient hiPSCs into mature myocytes in a highly efficient and reproducible manner and recapitulated some aspects of the disease phenotypes of CPT II deficiency in the myocyte disease models. This approach addresses the challenges of modeling the abnormality of FAO in CPT II deficiency using iPSC technology and has the potential to revolutionize translational research in this field.

1. Introduction

β-Oxidation of long-chain fatty acids (LCFA) occurs in the mitochondria with the activity of carnitine palmitoyltransferase II (CPT II; EC2.3.1.21), carnitine-acylcarnitine translocase (CACT), CPT I, and acyl-coenzyme A (CoA) synthetase. These enzymes mediate LCFA transport from the cytosol into the mitochondria. In response to conditions with a high-energy demand, such as intensive exercise, severe infection, and fasting, LCFA transfer is promptly activated [1–4]. *CPT2* maps to chromosome 1p32, spans 20 kb, contains five exons, and encodes the CPT II enzyme. Defects in CPT II enzymatic activity are classified into three clinical categories in humans: lethal neonatal (MIM #608836), severe infantile (MIM #600649), and mild adult-onset (MIM #255110) types. Due to the low enzymatic activity of CPT II, the neonatal and infantile forms result in liver failure, hypoketotic hypoglycemia, and cardiomegaly. The neonatal form causes death within several months. The infantile form has been implicated in cases of sudden infant death syndrome. On the other hand, the adult-onset type

* Corresponding author. Address: Division of Nephrology and Rheumatology, Department of Internal Medicine, Fukuoka University School of Medicine, 7-45-1 Nanakuma, Jonan-ku, Fukuoka, Fukuoka 814-0180, Japan. Fax: +81 92 873 8008.
E-mail address: yasuno9584@fukuoka-u.ac.jp (T. Yasuno).

http://dx.doi.org/10.1016/j.bbrc.2014.04.084
0006-291X/

manifests as recurrent myalgia (muscle pain), rhabdomyolysis, and myoglobinuria, which can cause acute renal failure. CPT II deficiency is generally considered an autosomal recessive disease; however, many cases of symptomatic carriers have been reported [5]. Individuals who carry a *CPT2* mutation [6–9] may develop the clinical features of CPT II deficiency when treated with medications that affect the activity of the remaining wild-type CPT II enzyme.

In this study, we successfully derived human induced pluripotent stem cells (hiPSCs) from a patient with CPT II deficiency, differentiated them into a mature myocyte lineage within 2 weeks in a highly efficient and reproducible manner, and recapitulated some of the disease phenotypes associated with CPT II deficiency. We discuss the opportunities to use iPSC technology for modeling defects in FAO and for evaluating therapeutic regimens for CPT II deficiency.

2. Patient and methods

2.1. Patient

The subject of the current study was a 24-year-old Japanese man whose genetic and clinical presentation has already been described [10]. The patient suffered from acute renal failure induced by rhabdomyolysis and was diagnosed as having adult-onset CPT II deficiency. Skin biopsy samples were obtained from the patient with his written informed consent. This study was approved by the Ethics Committee on hereditary disease, Research of the Graduate School of Medical Sciences, Fukuoka University, and by the Ethics Committee of Kyoto University. The dermal fibroblasts were expanded from skin biopsy explants in Dulbecco's modified Eagle's medium (DMEM; Nacalai Tesque, Kyoto, Japan) supplemented with 10% fetal bovine serum (Japan Bioserum, Hiroshima, Japan). Control iPSCs (201B7) were previously established from the facial dermis of a 36-year-old Caucasian woman at the Center for iPS Cell Research and Application (CiRA), Kyoto University [11].

2.2. Methods

2.2.1. Generation of hiPSCs from the patient

CPT II deficiency-specific hiPSCs were derived from the patient by transducing the four reprogramming factors (OCT4, SOX2, KLF4, and c-MYC) or three factors (excluding c-MYC) into skin fibroblasts with retrovirus vectors as previously described [11,12]. In brief, fibroblasts derived from the CPT II-deficient patient were maintained and expanded in DMEM containing 10% fetal bovine serum. The patient fibroblasts were seeded in 6-well plates at 1.0×10^5 cells/well. The next day, the cells were infected with Slc7a1 lentiviruses with 4 μg/mL polybrene (Nacalai Tesque). Fibroblasts expressing the mouse Slc7a1 were seeded in 6-well plates at 1.0×10^5 cells/well 1 day before transduction. Equal amounts of four retrovirus-containing supernatants were mixed and supplemented with 4 μg/mL polybrene. Six days after transduction, the fibroblasts were replated onto mitomycin C-treated SNL feeder cells. Thirty days after transduction, iPSC colonies were selected for expansion.

2.2.2. Cell culture

CPT II-deficient hiPSCs were cultured as previously described [11]. The hiPSCs were grown on mitomycin C-treated SNL feeder cells in Primate ES medium (ReproCELL, Kanagawa, Japan) supplemented with 500 U/mL penicillin/streptomycin (Invitrogen, Carlsbad, CA) and 4 ng/mL recombinant human basic fibroblast growth factor (bFGF, Wako, Osaka, Japan). For routine passaging, hiPSC colonies were dissociated by an enzymatic method with CTK dissociation solution consisting of 0.25% trypsin (Invitrogen), 0.1% collagenase IV (Invitrogen), 20% knockout serum replacement (KSR, Invitrogen), and 1 mM $CaCl_2$ in PBS (Nacalai Tesque) and split at a ratio between 1:3 and 1:6.

2.2.3. Embryoid body (EB) formation

For EB formation, a 10-cm plate containing hiPSCs was rinsed with PBS and treated with 1 mg/mL type IV collagenase (Invitrogen) in DMEM for 10 min at 37 °C. The collagenase was rinsed away with PBS and replaced with undifferentiation medium. The cells were then scraped off with a cell scraper (IWAKI, Tokyo, Japan), dissociated by pipetting, and distributed into a low attachment 6-well plate (Corning, Tokyo, Japan) containing knockout-DMEM (Invitrogen) supplemented with 20% KSR, 0.1 mM non-essential amino acids (Invitrogen), 2 mM glutamine (Invitrogen), 500 U/mL penicillin/streptomycin, and 0.55 mM 2-mercaptoethanol (Invitrogen). After 8 days as a floating culture, the EBs were transferred to gelatin-coated plates and cultured in the same medium for another 8 days.

2.2.4. Teratoma formation

The undifferentiated iPSCs were harvested using CTK dissociation solution, collected, and centrifuged, and the pellets were resuspended in DMEM/F12 (Invitrogen). A quarter of the iPSCs from a confluent 10-cm plate was injected into the testes of a non-obese diabetic/severe combined immunodeficient (NOD-SCID mouse, CLEA, Tokyo, Japan). Nine to 12 weeks after injection, the tumors were dissected and fixed with PBS containing 4% paraformaldehyde (PFA). Paraffin-embedded tissues were sectioned and stained with hematoxylin and eosin.

2.2.5. Mutational analysis of the CPT2 in patient-derived iPSCs

Overlapping PCR primers that targeted CPT2 exons were designed to cover the entire coding region (Table 1; GenBank accession No. M58581). The PCR protocol was as follows: 30 cycles of 1 min at 94 °C for denaturation, 1 min at 60 °C for annealing, and 1 min at 72 °C for extension, followed by 1 cycle of 10 min at 60 °C for completion. Each PCR product was sequenced on an automated DNA sequencer (ABI 3100 Genetic Analyzer; Applied Biosystems Hitachi, Tokyo, Japan) by using the BigDye Terminator v3.1 cycle-sequencing kit (Applied Biosystems, Foster City, CA) and the sequencing primers listed in Table 1.

2.2.6. Induction of hiPSCs into skeletal muscle cells

We used our previously reported method in which *MYOD1* overexpression in undifferentiated hiPSCs efficiently and reproducibly induces differentiation into mature skeletal muscle cells within 10 days [13]. Briefly, we transduced a self-contained Tet-inducible MYOD1 expressing *piggyBac* vector (Tet-MYOD1 vector) and transposase into CPT II-deficient iPSCs by lipofection. This system allows the indirect monitoring of induced *MYOD1* expression in response to doxycycline (Dox) by co-expression of a red fluorescent protein (mCherry). It was also reported that low glucose culture conditions purified the cardiomyocytes from mouse and human iPSC differentiation cultures by selecting only cardiomyocytes, based on the findings of the substantial biochemical differences in glucose and lactate metabolism between cardiomyocytes and undifferentiated iPSCs [14]. We used a similar strategy to increase the purity of generated myocytes and cultured the hiPSC-derived differentiated cells with low glucose media (1.0 g/L) for an additional day after 10 days of myocyte induction by *MYOD1* overexpression. The low-glucose medium was composed of MEM (Sigma, St. Louis, MO) containing 0.4% bovine serum albumin (Sigma), 0.4 mM L-carnitine (Sigma), 0.2 mM unlabeled palmitic acid (Nacalai Tesque), and 500 U/mL penicillin/streptomycin. For

Table 1
Oligonucleotide sequences, related to Fig. 1. Sequences of primers used in this study.

Gene	Forward primer: 5′ to 3′	Reverse primer: 5′ to 3′
hOCT4Tg	GCTCTCCCATGCATTCAAACTGA	CCCTTTTTCTGGAGACTAAATAAA
hSOX2 Tg	TTCACATGTCCCAGCACTACCAGA	GACATGGCCTGCCCGGTTATTATT
hKLF4 Tg	CCACCTCGCCTTACACATGAAGA	GACATGGCCTGCCCGGTTATTATT
hcMYC Tg	ATACATCCTGTCCGTCCAAGCAGA	GACATGGCCTGCCCGGTTATTATT
hOCT4 Total	CCCCAGGGCCCCATTTTGGTACC	ACCTCAGTTTGAATGCATGGGAGAGC
hSOX2 Total	TTCACATGTCCCAGCACTACCAGA	TCACATGTGTGAGAGGGGCAGTGTGC
hKLF4 Total	GATTACGCGGGCTGCGGCAAAACCTACACA	TTAAAAATGTCTCTTCATGTGTAAGGCGAG
hcMYC Total	ATACATCCTGTCCGTCCAAGCAGA	TCACGCACAAGAGTTCCGTAGCTGTTCAAG
CPT2 exon1	CGGCCTTGTGTTTAGACTCC	CTTCCAGATTAGGGGCTGTG
CPT2 exon2	GCCTTACACTGACCCTGCTT	AGGTTCTGGGTTCCTGGAGA
CPT2 exon3	TTCCAGGTTTTAGGGCTATG	GGAGGATGAGACGTTACTTC
CPT2 exon4	TAGGGACAGCATTAACATTT	TGGCCTTGTCATCAGTGAAG
CPT2 exon4	GTCCCAGTATTTTCGGCTTT	TGTGGGACAAGTGGACAAGG
CPT2 exon4	GAGTTTCCCCTGGCATACCT	GCCTCCTCTCTGAAACTGGA
CPT2 exon4	ACAGCTGCTAAGGAAAAGTT	CAAGACCCAAGGGCATGCTC
CPT2 exon5	CTGAGACGCTGGTTTTCCA	GGTAGCTTTTCATCTGCCCA

immunostaining analyses of hiPSC-derived myocytes, human myosin heavy chain (MHC) antibody (R&D Systems, Minneapolis, MN) was used according to the manufacturer's instructions. Samples were observed under an inverted type fluorescence phase-contrast microscope (BZ-9000E; Keyence, Osaka, Japan).

2.2.7. In vitro probe assay of AC profiles

hiPSC-derived myocytes were cultured in a 6-well plate for 96 h with 1 mL medium A composed of MEM, 0.4% bovine serum albumin, 0.4 mM L-carnitine, 0.2 mM unlabeled palmitic acid, and 1% penicillin/streptomycin without L-glutamine, or medium B composed of medium A supplemented with 0.4 mM bezafibrate (Sigma) [15]. Cultured cells were incubated with medium A or B at 38 °C for 96 h to determine the effects of heat stress on mitochondrial FAO.

2.2.8. Quantitative acylcarnitine analysis

Acylcarnitine in the culture supernatant was analyzed by MS/MS (API 3000; Applied Biosystems).

2.2.9. Heat stimulation

Differentiated myocytes on culture day 9 were subjected to heat stress at 38 °C on a hot plate.

2.2.10. Regulated PCR array for skeletal muscle-related genes

To analyze the expression of skeletal muscle-related genes, we performed a regulated PCR array. For first-strand cDNA synthesis, 1 μg total RNA was reverse-transcribed in a 20-μl reaction mix and the RT^2 First Strand Kit (RT^2 Profiler PCR Array, SuperArray Bioscience, Frederick, MD) according to the manufacturer's instructions. qRT-PCR was performed with a CFX96 (Bio-Rad, Hercules, CA) and universal cycling conditions (10 min at 95 °C, 15 s at 95 °C, and 1 min at 60 °C for 40 cycles). The fold change in gene expression was determined by the comparative cycle Ct (ΔΔCt) method. Statistical calculations were based on the web-based RT^2 Profiler PCR Array Data Analysis (SuperArray Bioscience).

2.2.11. Microarray analysis

aRNA preparation, fragmentation, hybridization, and scanning of the GeneChip Human Genome U133 Plus 2.0 Array (Affymetrix, Santa Clara, CA) were performed according to manufacturer's protocols. Labeled aRNA was prepared with the GeneChip 3′IVT Express Kit (Affymetrix). Briefly, cDNA was generated from total RNA (100 ng), using reverse transcriptase and a T7-oligo (dT) primer. After second-strand cDNA synthesis, the cDNA was converted to aRNA by an *in vitro* transcription reaction with biotin-labeled ribonucleotides and T7 RNA polymerase. After synthesis, the aRNA was purified to remove enzymes, salts, and unincorporated nucleotides. The concentration of cRNA was determined from the absorbance at 260 nm in a UV spectrophotometer. The aRNA was fragmented at 94 °C in fragmentation buffer (Affymetrix). The samples were hybridized to the GeneChip(R) Human Genome U133 Plus 2.0 Arrays at 45 °C for 16 h with rotation (60 rpm) in an oven. The arrays were automatically washed and stained with the GeneChip Hybridization, Wash and Stain Kit (Affymetrix). The Probe Array was scanned using a GeneChip Scanner 3000 7G (Affymetrix). Intensity data and the CHP files were generated by Affymetrix GeneChip Command Console Software and Affymetrix Expression Console Software.

3. Results

3.1. Generation of CPT II-deficient iPSCs (CPTIID-iPSCs) from patient fibroblasts

The skin fibroblasts were converted into iPSCs after transduction with four retroviral vectors encoding OCT4, SOX2, KLF4, and c-MYC, or with three vectors (excluding c-MYC). Quantitative reverse-transcription PCR was used to evaluate the CPTIID-iPSC clones with repression of the exogenously introduced genes analyzed as the ratio of transgene (Tg) expression to total (endogenous and transgene) expression (Table 1). Based on these analyses, the iPSC clone with the highest level of repression was selected for further experiments. This clone exhibited characteristic human embryonic stem cell (ESC) morphology (Fig. 1A), expressed pluripotency markers, including OCT4, NANOG, SOX2, SSEA4, TRA-1-60, TRA-1-81, and alkaline phosphatase (AP) activity (Fig. 1B), and had a normal karyotype (Fig. 1C). The pluripotent properties of CPTIID-iPSCs were also assessed using embryoid body (EB) and teratoma formation upon intratesticular injection of undifferentiated CPTIID-iPSCs into NOD-SCID mice (Fig. 2A and B). Genetic identity was confirmed by STR analyses of the patient fibroblasts and iPSCs (data not shown). Mutation analysis of the causative gene revealed that the patient had compound heterozygous mutations in the *CPT2* [10]. Genomic analysis showed that both CPTIID-iPSCs and their parental fibroblasts possessed mutant CPT2 alleles (Fig. 1D). Sequencing from the 5′ and 3′ ends showed a CT deletion in the TCT at codon 408 (1223delCT), resulting in a stop signal at codon 420, and a sense mutation of arginine to cysteine at codon 631 (1891C→T; R631C). These results suggest that disease-specific iPSCs can be generated from the skin fibroblasts of a CPT II-deficient patient.

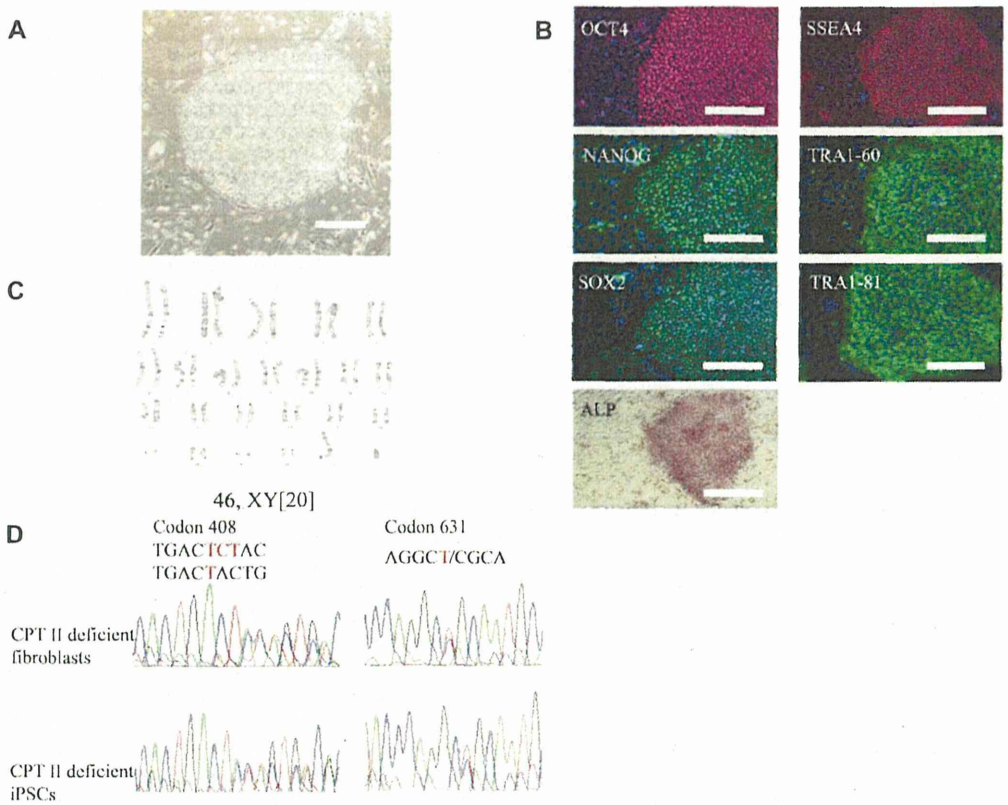

Fig. 1. Generation of iPSCs from a patient with CPT II deficiency. (A) Typical image of human embryonic stem cell (ESC)-like colony. Scale bars: 50 μm. (B) Immunocytochemistry for OCT4, NANOG, SOX2, SSEA4, TRA1-60 and TRA1-81, and the examination of alkaline phosphatase (AP) enzyme activity. Nuclei were stained with Hoechst 33342 (blue). Scale bars: 100 μm. (C) Karyotype analyses of CPT II-deficient iPSCs. (D) Mutational analyses of CPT II-deficient iPSCs and their parental fibroblasts. Sequencing from the 5′ and 3′ ends reveals a CT deletion from the TCT at codon 408, and an arginine to cysteine substitution at codon 631.

3.2. Differentiation of CPTIID-iPSCs into mature myocytes

We next examined whether the patient-derived iPSCs could be differentiated into myocytes, the target cell type of CPT II deficiency. We recently reported a highly efficient myocyte differentiation method based on overexpression of the *MYOD1* gene, a master regulator of myocyte lineage differentiation, in undifferentiated hiPSCs [13]. Tohyama et al. reported a non-genetic method for purifying cardiomyocytes in mouse and human iPSC differentiation cultures [14]. Their strategy is based on the substantial biochemical differences in glucose and lactate metabolism between cardiomyocytes and non-cardiomyocytes, including undifferentiated iPSCs. We used a combination of these strategies to generate myocytes from CPTIID-iPSCs. We transduced a Tet-MYOD1 vector and transposase into CPTIID-iPSCs by lipofection. We forced expression of *MYOD1* with Dox in undifferentiated CPTIID-iPSCs for 10 days. We then used low glucose medium for an additional day to select myocytes. After culture in low glucose medium, the remaining undifferentiated cells disappeared, and the differentiated cells survived, yielding myocyte generation at 50%–60% induction efficiency.

We confirmed the presence of mature myocytes by staining with anti-human MHC antibody (Fig. 3A). Electron microscopy revealed that differentiated myocytes derived from CPTIID-iPSCs had myofibrils containing mature myosin fibers and Z line-like structures (Fig. 3B). We also performed a PCR array and unsupervised clustering to generate myogenic gene profiles for myocytes differentiated from CPTIID-iPSCs, myocytes from control iPSCs (201B7), undifferentiated CPTIID-iPSCs, and undifferentiated 201B7 cells (Fig. 3C, Table 2). We confirmed the upregulation of markers of skeletal muscle contractility, skeletal myogenesis, and skeletal muscle autocrine signaling in myocytes differentiated from CPTIID-iPSCs compared to undifferentiated CPTIID-iPSCs. The expression patterns of muscle-related genes also differed between myocytes derived from CPTIID-iPSCs and control myocytes. These results suggest that mature myocytes can be efficiently generated from CPTIID-iPSCs by introducing a master transcriptional regulator of myocyte differentiation, MYOD1, and culturing in low glucose conditions.

3.3. Acylcarnitine (AC) profiles of the CPT II-deficient myocytes

An acylcarnitine profile determined by tandem mass spectrometry is essential for the definitive diagnosis of CPT II deficiency [15]. We thus examined the profile in myocytes differentiated from CPTIID-iPSCs. CPT II-deficient myocytes accumulated more C16 (palmitoylcarnitine) than did control myocytes (Fig. 4). Results were similar in myocytes differentiated from other iPSC clones from the same patient in this study (data not shown). These data indicated that patient-derived iPSCs recapitulated one of the clinical features of CPT II deficiency.

We previously reported that fibroblasts from patients with LCFA β-oxidation disorders, including CPT II deficiency, were more susceptible to heat stress in comparison to the fibroblasts of patients with medium-chain fatty acid β-oxidation disorders or healthy controls [15]. We thus investigated the effects of heat stress on myocytes derived from CPTIID-iPSCs and found that this treatment significantly increased C16 in CPT II-deficient cells, but not in controls (Fig. 4). We also demonstrated that bezafibrate, an agonist of peroxisome proliferator-activated receptor (PPAR), restores FAO activity in fibroblasts

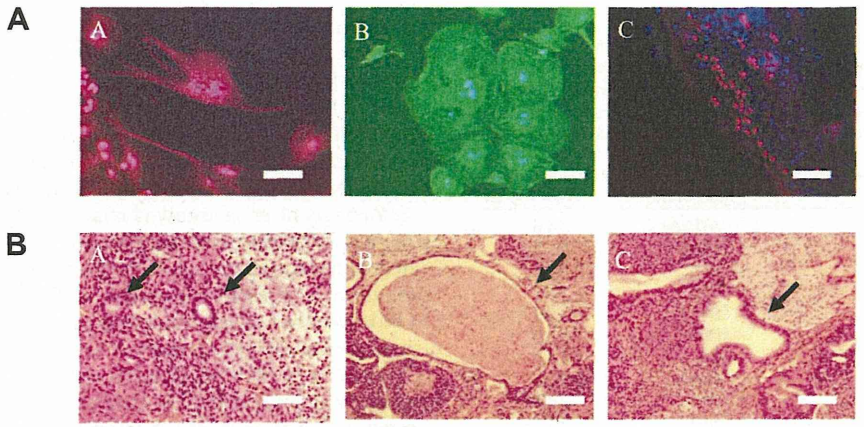

Fig. 2. Embryoid body (EB)- and teratoma-mediated differentiation of CPT II-deficient iPSCs. (A) Immunostaining of EBs generated from CPT II-deficient iPSCs for TUJ1 (ectoderm, A), α-SMA (mesoderm, B), and SOX17 (endoderm, C). Nuclei were stained with Hoechst 33342 (blue). Scale bars: 100 μm. (B) Hematoxylin and eosin staining of histological sections of teratomas derived from CPT II-deficient iPSCs. Neural tissues (ectoderm, A), cartilage (mesoderm, B), gut-like epithelia (endoderm, C). Scale bars: 100 μm.

with CPT II deficiency [15]. We investigated the effects of bezafibrate on myocytes derived from CPTIID-iPSCs. At 37 °C and 38 °C, bezafibrate decreased C16 levels in controls and CPT II-deficient myocytes. In the CPT II-deficient myocytes, bezafibrate at 37 °C reduced C16 levels to those observed in controls (Fig. 4). These results suggest that mature myocytes derived from CPTIID-iPSCs recapitulate some of the phenotypes associated with CPT II deficiency.

4. Discussion

Rhabdomyolysis occurs after exhaustive exercise or severe infection without trauma or drugs in CPT II deficiency. The adult-onset form presents with myoglobinuria and myalgia, frequently leading to acute renal failure. Rhabdomyolysis may repeatedly develop within the same families. Hereditary rhabdomyolysis is often caused by compromised enzymatic activity associated with LCFA metabolism.

Accurate experimental modeling of the disease and its response to clinical intervention are hampered due to a lack of appropriate animal models. To address this issue, we sought to derive iPSCs from a patient with CPT II deficiency, who had a history of repetitive rhabdomyolysis and acute renal failure. There have been no reports of derivation of iPSCs from patients with FAO disorders, including CPT II deficiency, and to the best of our knowledge, we are the first to report the successful generation of iPSCs from a CPT II-deficient patient.

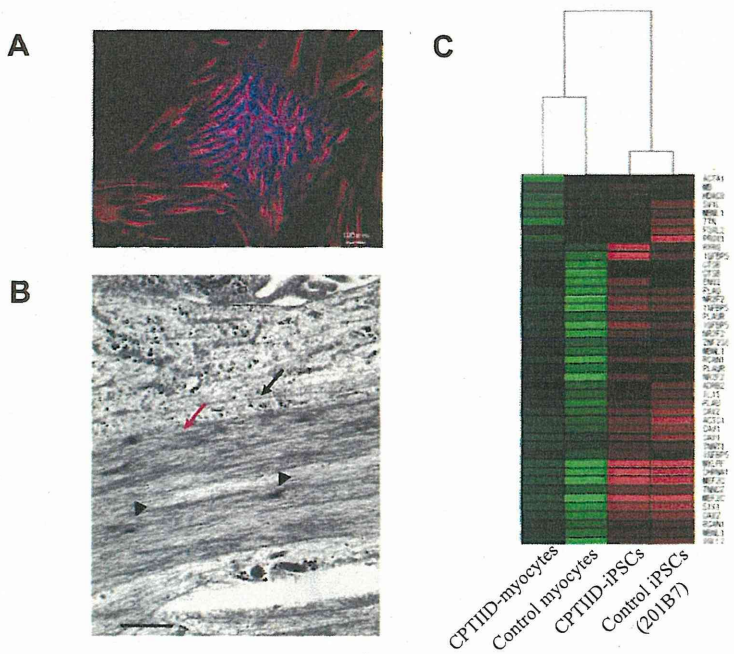

Fig. 3. Directed differentiation of CPT II-deficient iPSCs into skeletal muscle cells. (A) Immunocytochemistry of the myocytes derived from CPT II-deficient iPSCs with anti-human Myosin Heavy Chain (MHC) antibody. Nuclei were stained with Hoechst 33342 (blue). Scale bar: 100 μm. (B) Structural analysis of myocytes differentiated from CPT II-deficient iPSCs by electron microscopy. A red arrow indicates myofibrils. Black arrowheads indicate immature Z lines. A black arrow indicates myosin fibers. Scale bar: 500 nm. (C) Characterization of iPSC-derived myocytes. Myogenic gene profiles and unsupervised clustering based on markers associated with myocytes in undifferentiated iPSCs and differentiated myocytes. CPTIID-myocytes, control myocytes, CPTIID-iPSCs, and control iPSCs. Green indicates up-regulated genes and red indicates down-regulated genes. Up-regulated genes were identified by changes of at least 2-fold. CPTIID-myocytes; Myocytes differentiated from CPTIID-iPSCs.